CHAPTER 8

Traps and Interfaces in Photocatalysis: Model Studies on TiO_2 Particle Systems

THOMAS BERGER[a] AND OLIVER DIWALD*[a]

[a]University of Salzburg, Department of Chemistry and Physics of Materials, Hellbrunnerstrasse 34/III, A-5020 Salzburg, Austria
*E-mail: Oliver.Diwald@sbg.ac.at

8.1 Introduction

Nanoparticulate TiO_2 is the prototypical materials system for research on disperse systems for solar energy conversion and photocatalysis. It is therefore surprising how many open issues and controversial points have remained in trying to reach reliable predictions for newly designed TiO_2 based materials and their functional properties. Our still limited knowledge of nanoscale effects and the chemistry and photochemistry thereof complicate the systematic improvement of TiO_2 particle based materials.[1,2] At the same time, it still encourages more research on TiO_2 based model systems. However, the impact of factors underpinning the photocatalytic activity of a given semiconductor material is complex and convoluted. One current idea in the scientific literature is that there are too many intermingled factors that are associated with the photophysics, surface chemistry, as well as with the defect properties, to arrive at a scientifically sound concept for the rational

RSC Energy and Environment Series No. 14
Photocatalysis: Fundamentals and Perspectives
Edited by Jenny Schneider, Detlef Bahnemann, Jinhua Ye, Gianluca Li Puma, and Dionysios D. Dionysiou

Published by the Royal Society of Chemistry, www.rsc.org

design and optimization of photocatalyst materials.[3–7] It seems that this idea increasingly gains ground. Thus, the question – being relevant to the entire field of catalysis research – is whether conclusions from photoexcitation studies, which have been carried out on model materials of reduced compositional and structural complexity, can ever be general enough to be linked to working catalysts in a relevant way (Figure 8.1).

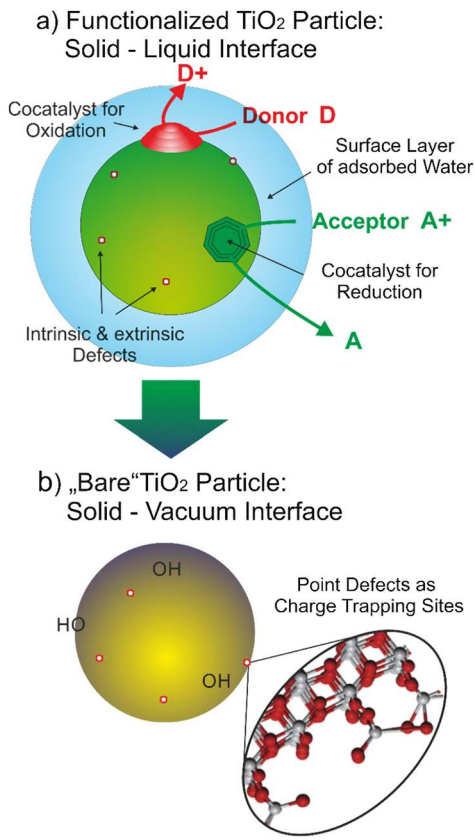

Figure 8.1 Simplified scheme illustrating the decrease of materials complexity associated with the transformation of a composite particle based photocatalyst (a) with (i) functional components such as co-catalysts and (ii) surrounded by electron and hole scavengers that are adsorbed at the particle surface or dissolved in the surrounding liquid (D and A^+) into a bare and uncapped TiO_2 particle the surrounding continuous phase of which was ultimately replaced by a gas or vacuum phase (b). Even after materials processing in vacuum performed to eliminate surface layers of adsorbates, a TiO_2 particle of type (b) still hosts defects with functional as well as unwanted properties such as ion vacancies, interstitials and adsorbates that all may act as charge trapping sites. The question arises whether insights from model studies performed on TiO_2 particle systems with relatively defined surface and interface properties (b) will ever connect to performance data obtained on a working photocatalyst (a).

TiO_2 based particles that show activity for photocatalytic water splitting are typically described as functional composites which involve (i) a photon absorber (*e.g.* the semiconductor), (ii) a reduction co-catalyst (*e.g.* for hydrogen evolution) and (iii) an oxidation co-catalyst (*e.g.* for oxidation evolution from water) (Figure 8.1(a)).

For photocatalytic water splitting the separation and transfer of photogenerated charge carriers, the suppression of charge carrier recombination and finally the enhancement of photocatalytic activity are promoted by TiO_2 functionalization with co-catalysts. The electrochemical description of semiconductor particles as short-circuited microelectro-chemical cells implies that there are always two conjugate half-reactions that have to be taken into account.[2,4] These half-reactions relate to the fate of photogenerated electrons and holes and determine the mixed photopotential. In the absence of both co-catalysts and reactants the nature and composition of the interface (Figure 8.1, solid–gas *versus* solid–liquid) determine the nature of the charge trapping sites available and, thus, associated particle charging effects.

Researchers from the surface science community performing experiments on solid surfaces that are well-defined in terms of composition and surface structure typically put forward the idea that the development of effective strategies for efficient photochemical processes requires an understanding of the elementary steps that lead to the overall reaction.[8–11] Related efforts would involve the characterization of surface as well as adsorbate structures, the identification of photo-active intermediates on the surface and a description of surface defects that undergo in the course of a photoinduced surface process changes in electronic structure.

To approach this explicit model situation with particle based materials one would need to identify disperse model systems that are well-defined with regard to chemical composition and structure. In addition, these particle systems should exhibit narrow size distributions and sufficient thermal stability to survive surface purification treatment *via* thermal activation in selected gas atmospheres without particle coarsening and coalescence.[12]

This chapter is organized as follows: in the first part we will outline selected efforts to characterize on TiO_2 nanoparticles with bare and essentially dehydroxylated particle surfaces characteristic spectroscopic features and fingerprints that are related to trapped charge carriers. This part will also include insights and understanding from recent *ab initio* calculations. Then, in the second part, we will describe the evolution and build-up of spectroscopically accessible charging states that can be tracked by methods such as electron paramagnetic resonance (EPR), FT-IR and photoluminescence (PL) spectroscopy under continuous UV exposure. Underlying processes typically saturate at a certain level that corresponds to a specific concentration of separated electron and hole centers.[13,14]

Upon immersion of dry particle systems into liquid dispersing agents and their transformations into colloidal systems solid–gas interfaces become replaced by a solid–liquid interface and the materials situation gains substantially in complexity. However, photo-electrochemistry can come into play

and – in addition to its potential to quantify transferred charges – it can shed light on an additional charge redistribution process, *i.e.* on the redistribution of protons inside an immobilized ensemble of TiO_2 nanoparticles (see below). Finally, we will address an important but largely overlooked issue that is inherent to particle systems dispersed in liquid as well as gaseous continuous phases. Aggregation and disaggregation and – concomitantly – the formation or break up of solid bridges between particles does occur during different particle processing steps as well as under photocatalytic operation during UV excitation.[15–17] With regard to their impact on the photo-activity of highly dispersed photocatalysts the formation and break up of particle–particle interfaces critically affect transport as well as recombination of photogenerated charges.

8.2 The Solid–Gas Interface: Trapping Sites and Spectroscopic Manifestations

Different radical intermediates can emerge from photoexcitation of TiO_2 particle systems.[18–21] Among them photogenerated electrons and electron hole centers, which are subject to subsequent trapping at defect sites, are employed as site selective surface probes and accessible to electron paramagnetic resonance (EPR) as a particularly insightful analytical technique.[22–27] The EPR technique allows one to map out the electron density in the vicinity of a paramagnetic trapping site, to identify distortion of neighboring atoms around the defect and to probe the internal electric and magnetic fields at the trapping site. This is also true for molecular radicals derived from these charge carriers. The main paramagnetic sites which emerge upon UV excitation of dehydroxylated TiO_2 particles and which have been isolated on their surface or inside their bulk are listed in Table 8.1.

8.2.1 Trapped Electrons

Historically, EPR work directed to semiconductor photocatalysis started on frozen TiO_2 colloids. Characteristic types of $Ti^{3+}(d^1)$ centers, the EPR powder signals of which exhibit a relatively narrow linewidth and which are characterized by g tensor components of $g_{\parallel} = 1.990$ and $g_{\perp} = 1.960$, were found to be essentially independent of the pH of the surrounding dispersion agent.[38] The insensitivity of the EPR line width to deuteration of the colloid surface was explained by the respective trapping sites' location in the interior of the anatase particle.[39] This outcome actually resembles a situation where hydrogen is used as an external electron source. Related charge separation processes can be engaged when dry TiO_2 particle powders become exposed to (i) atomic hydrogen or (ii) are UV excited in the presence of molecular hydrogen which serves as an hole scavenger under such conditions.[39] Again, replacement of hydrogen by deuterium atoms does not show any isotope effect (H: $I = 1/2$, D: $I = 1$) on line shape and signal splitting. This points to the fact that the

Table 8.1 Paramagnetic sites observed on dehydroxylated anatase TiO_2 particle systems during or after UV excitation.

Paramagnetic site	Electron configuration	Chemical reactivity at room temperature and below	References
Ti^{3+}[I] $g_\perp = 1.9640/g_\parallel = 1.9495$	$3d^1$	Electron transfer to O_2	28–30
Ti^{3+}[II] $g_\perp = 1.9900/g_\parallel = 1.9600$			
Electron center $g_{iso} = 2.0025$	Unknown	No surface reactivity reported	16 and 31
Trapped electron hole O– $g_\perp = 2.0121/g_\parallel = 2.0046$	$2p_x^2 2p_y^2 2p_z^1$	Cleaving of H–H, –C–H, –C–C– and –C–Si– bonds; reaction with O_2 to ozonide-type trinuclear oxygen adducts	22,27,28,32
Oxygen radicals			
O_2–[I] $g_{zz} = 2.0248/g_{yy} = 2.0096/g_{xx} = 2.0033$	$(1\sigma_g)^2(1\sigma_u)^2(2\sigma_g)^2(2\sigma_u)^2$ $(3\sigma_g)^2(1\pi_u)^4(1\pi_g)^3$	CO oxidation	28,33–36
O_2–[II] $g_{zz} = 2.0184/g_{yy} = 2.0096/g_{xx} = 2.0033$	$(1\sigma_g)^2(1\sigma_u)^2(2\sigma_g)^2(2\sigma_u)^2$ $(3\sigma_g)^2(1\pi_u)^4(1\pi_g)^3$		
O_3–[I] $g_\perp = 2.0015/g_\parallel = 2.0073$	$(1a_2)^2(2b_2)^2(3a_1)^2(2b_1)^1$	CO oxidation	28,34,35,37
O_3–[II] $g_\perp = 1.9996/g_\parallel = 2.0073$	$(1a_2)^2(2b_2)^2(3a_1)^2(2b_1)^1$		

spin density of the paramagnetic defect is negligibly small at the neighboring proton (or deuteron) of an adjacent hydroxyl group. Additional experiments to address potential hyperfine interaction arising from ions of the anionic sublattice were performed on TiO_2 particle systems which had been surface enriched with ^{17}O ($I = 5/2$). Corresponding results suggest that most trapped charges (*i.e.* Ti^{3+}) actually remain on the surface, whereas only a minority seems to stabilize in the sub-surface region of the particle.[30]

In TiO_2 aerosol nanoparticles which were synthesized and processed in dry atmosphere and measured under water-free conditions the *g* factors for the Ti^{3+} center are in qualitative agreement with those reported for colloids. The lower symmetry of the spin center's *g* tensor, however, reveals some differences in the local symmetry of the trapping site. Despite these changes in unit cell distortion, the comparison of EPR results obtained on frozen aqueous colloids and TiO_2 particle powders under vacuum conditions reveals a broad agreement. This is somehow surprising, since for metal oxide particle systems that are covered with water molecules and exhibit a substantial surface hydroxylation one would expect different trap sites with paramagnetic as well as diamagnetic properties as compared to TiO_2 nanoparticles with essentially bare oxide surfaces.

A recent perspective on the EPR characteristics of charge trapping sites in TiO_2 has been given by Giamello *et al.*[30] Particular attention has been paid to *g*-tensor analysis as well as to the important issue of hyperfine interaction and electron spin density using advanced pulse-EPR techniques. For a systematic comparison of trapped electrons in the TiO_2 polymorphs anatase and rutile the authors employed different chemical and physical procedures – such as (i) the admixture of aliovalent ions (*e.g.* Nb^{5+} or F^-) to the TiO_2 lattice during synthesis, (ii) the exposure of particle powders to H atoms and (iii) the photoexcitation of particle powders in the presence of hole scavengers, such as molecular H_2. Despite the structural complexity of a particle ensemble and in particular the analytical challenge of site heterogeneity the authors identified EPR powder signals with well-defined EPR parameters. These also include hyperfine data obtained on ^{17}O ($I = 5/2$) enriched samples. The two predominant cases, discussed by the authors, are interstitial Ti sites in rutile and substitutional Ti sites in anatase. In the case of TiO_2 rutile the measured spin density at the six oxygens around the $Ti^{3+}(d^1)$ cation clearly points to a single cation as a spin center,[40] while delocalization must be inferred from the respective data of TiO_2 anatase.

In semiconducting metal oxides oxygen deficiency typically connects to defects that are also likely candidates for charge trapping. For this reason, oxygen vacancies and associated excess electrons have been extensively examined by theory.[41–43] Consistent with their experimental observation by surface science techniques – *i.e.* a defect feature approximately 1 eV below the conduction band minimum as seen by ultraviolet photoelectron spectroscopy (UPS) and electron energy loss (EELS) spectroscopy – modern hybrid density functional calculations correctly reproduce the presence of localized defect states detached from the bottom of the conduction band. For the

rutile modification of TiO_2 most of the associated spin density is localized on the two Ti ions adjacent to the oxygen vacancy, which leads to the electronic reduction of Ti^{4+} ions to Ti^{3+} ions. The relaxed singly charged oxygen vacancy with one unpaired electron corresponds to a trapped state localized at a six-fold coordinated cation. This is quite different from other prototypical semiconducting oxides such as ZnO and WO_3 where the excess electron density was found to be localized at the vacancy site,[43] a situation which is comparable to F^+ centers in strongly ionic insulating metal oxides or halides. While for TiO_2 it is still debated whether trapped electrons are localized on single titanium cations[40] or delocalized over multiple ions, there appears to be agreement in the solid state physics and surface science community that the electronic structure of an oxygen vacancy does not provide sufficient stabilization to allow for electrons trapped inside the center of the defects.[9,43]

Interestingly, therefore, there are continued reports of single electron trapped oxygen vacancy centers,[44] also denoted as F^+ sites or color centers.[45,46] Isotropic EPR signals in the *g* value range between the free spin value $g = 2.0023$ and $g = 2.004$ are typically used as spectroscopic evidence for this defect type. Related paramagnetic electron centers, which do not undergo an electron transfer to adsorbed O_2, have been reported for TiO_2-based materials for many years. Serwicka *et al.*[47] found that on oxygen deficient TiO_2 the adsorption of electron acceptors such as O_2, SO_2 or SF_6 leads to an intensity increase of a symmetrical signal at $g = 2.003$. This effect has been attributed to conduction band electrons localized at anion vacancy sites. In addition to other reports focusing on the optical properties of the underlying defects[48–50] some investigations even claimed a correlation between this type of center and photocatalytic activity in the visible light range.[45,51] Most reports, however, provide no or only very little information about the structural properties of the particle ensemble investigated and in particular about their level of particle agglomeration and aggregation. As will be outlined in more detail below, sample history, *i.e.* the way the TiO_2 particles were synthesized and subjected to thermal processing and sintering, is key to the generation and depletion of functional defects that determine the photo-electronic properties of materials.

In the past we characterized vapor phase grown TiO_2 particles before and after aggregation in great detail and observed the above described paramagnetic defect exclusively on ensembles of aggregated and sub-stoichiometric particles.[16,31] As an additional characteristic of this paramagnetic fingerprint, its intensity and resonating field also depend on residual oxygen in the surrounding gas atmosphere. The microwave saturation behavior proves that this electron center is chemically different from paramagnetic coke impurities which typically arise from annealing of oxide samples that are contaminated by synthesis related organics. Moreover, it was found that the underlying paramagnetic sites are isolated defects in the particles' subsurface region.[16] On the other hand, the defect must be close enough to the surface to feel the influence of adsorbed oxygen which induces a strong intensity increase of the associated signal.[16] A more detailed investigation addressing

the location of the underlying defect site would also involve theoretical modeling and is still missing. In any case, it can be concluded at this stage that in addition to well-accepted Ti^{3+} sites with characteristic *g* tensor components there also exist paramagnetic electron centers which directly connect to the presence of particle–particle interfaces and grain boundaries.[16] Up to now we did not observe any UV induced concentration changes, *i.e.* effects which would indicate their involvement in photophysical processes relevant to photocatalysis. Oxygen gas addition to nonstoichiometric TiO_{2-x} or to TiO_2 under UV excitation initiates transfer from Ti^{3+} states to adsorbed oxygen upon formation of surface adsorbed superoxide anions. Consequently, the Ti^{3+} signature in the EPR spectrum becomes annihilated.

8.2.2 Trapped Holes

The photo-oxidative properties of TiO_2 particle systems arise from photogenerated hole centers from the valence band or out of a trapped state (O^- radicals).[52] In addition to transient absorption spectroscopy,[15,53] EPR is the method of choice to explore hole trapping in metal oxide particle systems.[27,54,55] In TiO_2 particle systems photogenerated hole centers become predominantly trapped at the surfaces of the particles.[12,39] It is important to recall at this point that EPR signals of surface paramagnetic states and adsorbates are subject to quenching by molecular oxygen from the surrounding gas atmosphere. This effect, which originates from exchange interaction between the paramagnetic centers and triplet oxygen, provides an important diagnostic in order to discriminate between the spin center's location in or underneath the particle surface. Moreover, in the case of surface trapped hole centers (see below) this effect is indicative of oxygen content and the composition of the surrounding atmosphere. Thus, the measured intensity and line-shape of their related EPR signals (O^-: $g_\perp = 2.0121$, $g_\parallel = 2.0046$) is, first of all, subject to the residual gas atmosphere during spectroscopic measurement as well as to the general particle surface properties, *e.g.* total surface area, level of hydroxylation and hydration. There are different reports for dehydroxylated TiO_2 particle systems in controlled gas environment revealing O^- radicals generated from lattice O^{2-} in the valence band.[26,30,55,56] Despite first published results on ^{17}O enriched TiO_2 powders samples[57] the understanding of the local geometry of various surface trapping sites is less clear than in the case of Ti^{3+}. A certain controversy regarding trapped holes assignments mainly results from the fact that holes are localized in the TiO_2 surface region and highly reactive. As such they are able to cleave H–H, –C–H, –C–C– and –C–Si– bonds.[21,27,58] Moreover, we note that the role of hydroxyl groups becomes complicated also in this context, since under real photocatalytic conditions TiO_2 particle systems with surface hydroxyls and multilayers of adsorbed water are used. Under these conditions, there are large numbers of different hydroxyls which are embedded in different structural environments and which transform trapped hole centers in short-lived OH· radicals. These can only be tracked by spin trapping techniques which in turn require

a liquid solvent and, thus, would describe a solid–liquid interface.[59,60] From this it becomes clear that more work is still needed to unravel the mechanistic impact of surface hydroxyls and water molecules on the reactive pathway of photogenerated hole centers.

8.2.3 Trapped Hydrogen

Hydrogen impurities in semiconductor oxides have been the subject of intense and growing research activities.[61–64] For experiments, FT-IR spectroscopy has turned out to be an extremely sensitive and versatile technique not only to characterize the vibrational modes of H bond moieties inside the lattice but also to detect free and shallow trapped electrons.[64–67] Broad IR absorption signals typically emerge upon dissociation of molecular hydrogen on ZnO powders at 298 K[66,68] with intensities that increase with temperature.[69] These absorptions, the envelope shape of which was found to depend on particle morphology, were attributed to inter-band transitions of conduction band electrons and to electronic transitions from shallow donor states into the conduction band.[68] Similar experimental observations were made for ZnO that, prior to measurement, had either been contacted with atomic hydrogen[66] or exposed to a hydrogen plasma.[70] It was proposed that hydrogen atoms diffuse into grain boundaries and reach subsurface and bulk regions of the metal oxide where they become active as shallow donor states. In some oxides hydrogen is stabilized both in the form of ions and neutrals.[62] Using nuclear reaction analysis Traeger *et al.*[71] determined in commercially available ZnO single crystals hydrogen concentration levels that were significantly higher than those typically reported for shallow donor species. This underlines the substantial storage capacity of the metal oxide lattice for neutral atomic hydrogen.

A broad signal in the IR range, monotonically increasing towards lower wavenumbers, was observed after exposure of TiO_2 nanoparticles to atomic hydrogen gas or upon hydrogen dissociation and spillover on Au/TiO_2 nanoparticles.[72,73] In both cases hydrogen atoms presumably diffuse into the TiO_2 bulk and donate electrons to shallow trapped states. Both electron excitation from these states to the conduction band and inter-conduction band transitions have been proposed to contribute to the overall intensity of the broad IR signal measured under high vacuum conditions.[72,73] That H-doping produces Ti^{3+} species as a result of hydrogen atom dissociation into protons bound to a lattice oxygen and electrons has also been confirmed by recent DFT calculations.[63] Sezen *et al.*[67] explored the IR-absorption properties of rutile TiO_2 powders and single crystals and – after exposure to atomic hydrogen – presumably identified transitions of self-trapped conduction band electrons (intrinsic trap states) into excited hydrogenic states which correspond to polarons. As mentioned above, electron injection from hydrogen atoms into TiO_2 powders is also accessible to EPR spectroscopy as paramagnetic $Ti^{3+}(d^1)$ states upon hydrogen ionization.[30,39,43] For TiO_2 anatase powders the n-type doping level of the starting material seems to determine the relative

abundance of different types of Ti^{3+} species.[74] One type of Ti^{3+} center was exclusively formed in the anatase TiO_2 bulk when Nb doping was performed for valence induction.[30] On bare anatase TiO_2 powders that are exempt from dopants an additional Ti^{3+} center with a large line width was attributed to trapping sites at the semiconductor surface.[74] Whether the formation of bulk centers is (i) connected to surface ionization and electron diffusion towards the respective trapping site or (ii) to the penetration of neutral H atoms into the interior of the TiO_2 nanocrystal and subsequent ionization depends on temperature and has not been resolved up to now.[39] Upon heating of a H-covered sample, however, hydrogen diffusion into the rutile TiO_2 bulk was found to be favored in comparison to hydrogen elimination *via* desorption into the vacuum.[75] The relevance of subsurface sites for the trapping of hydrogen has been recognized both by theory and experiment.[76,77]

In addition to vacuum experiments, IR absorptions originating from electrons in shallow traps have also been measured in aqueous solutions. Related observations were made on TiO_2 during UV excitation in contact with hole acceptors dissolved in aqueous solutions[78,79] as well as during cathodic polarization in aqueous electrolytes.[80,81] The electrochemical electron accumulation in TiO_2 particle based electrodes in aqueous environment is connected to H atom ionization in vacuum insofar as the processes of electron localization and proton adsorption or proton insertion must occur in parallel.[82–84] This will be outlined in more detail in Section 8.6. Importantly, hydrogen is ubiquitous not only during the operation of the photocatalyst but also during material synthesis and characterization. Hydrogen is for instance the predominant residual gas in ultrahigh vacuum systems employed for surface science studies. In view of materials optimizations, this prompts the need for a more comprehensive exploration of hydrogen interaction with semiconductor oxides and its static and dynamic function therein.

8.2.4 Trapped Charges and Optical Fingerprints

The optical fingerprints of trapped charges have extensively been exploited in transient spectroscopy studies to follow the kinetics of elementary processes in a photocatalyst material upon UV exposure.[1,15] While trapped holes and electrons absorb light in the visible and NIR range, free electrons give rise to characteristic absorptions in the IR and MW range. A very broad signal is in the vis/NIR typically emerges from trapped electrons upon induced charge carrier separation,[85–88] thermal reduction,[89,90] injection of radiolytically generated hydrated electrons[91] or electrochemical charge accumulation.[92] This absorption has been attributed to electrons localized in band gap states (Ti^{3+} centers), to electrons in the CB, or to a superposition of both. The leveling off of the absorbance at longer wavelengths in the visible and NIR range, which in some cases culminates in a pronounced maximum, has been interpreted in terms of d–d transitions of localized Ti^{3+} states.[93,94] The d–d transition is symmetry forbidden, however, symmetry breaking by asymmetric ligand field splitting or vibronic coupling makes weak absorption possible.

The monotonic increase towards longer wavelengths, on the other hand, was attributed to the Drude absorption of free CB electrons.[95] Free electron transitions in the CB require an additional interaction to conserve momentum. The change in momentum can be provided by coupling with phonons or by scattering at impurities. Free CB electrons will give rise to a broad IR signal with an absorbance A developing as:

$$A(\lambda) = C\lambda^p \tag{8.1}$$

Here λ is the wavelength (in μm) and C is a proportionality constant. The scattering constant p can range from 1.5 to 3.5 depending on the statistical weight of the processes, which provide the momentum change. Broad IR absorptions typically observed on TiO_2 samples following UV exposure,[78,79,96,97] connected with atomic hydrogen,[67,98,99] electrochemical electron accumulation[80] or thermal reduction in vacuum,[97] have been assigned alternatively to inter-conduction band transitions, electron excitation from shallow-trapped states to the conduction band or transitions of self-trapped electrons into excited hydrogenic states corresponding to a polaron.

8.3 Slow Charge Trapping and Charge Carrier Quantification at the Solid–Gas Interface

In addition the bulk properties photocatalyst particle assemblies are characterized by various exposed crystal faces, which give rise to surface defects of different nature, energy and location. Upon light-induced charge carrier generation, these defects may act as sites for trapping, recombination or transfer of charge carriers. In this context, synergistic effects can occur between different surface planes with regard to trapping and consumption of electrons and holes.[100–102] However, after charge carrier generation, they have to be transported to the respective active sites. In TiO_2 particle assemblies such a transport is connected to multiple trapping events involving different trapping sites with a certain energetic and spatial distribution.[103] As a result, charge carriers undergo a sequence of consecutive steps until a steady state distribution of charge carriers is established.

Time-resolved absorption spectroscopy following laser pulse excitation has extensively been used to study charge carrier dynamics in photocatalyst particles.[1,2,15] This approach allows for tracking the elementary steps of charge carrier trapping (typically in the ps-range and below),[104] charge carrier recombination (typically in the ps- to ns-range) as well as fast interfacial charge transfer (typically in the sub-ns to ms range). However, the time to reach at a given light intensity a steady state with respect to the energetic and spatial distribution of trapped charges can exceed the duration of a single laser pulse as applied in transient spectroscopic studies.

In situ time-dependent spectroscopic information about light induced processes which occur on the time scale of minutes and above, as well as under

continuous wave excitation using low light irradiances (in the power range of mW cm^{-2}) are scarce. Such conditions, however, resemble the situation typically encountered in photocatalysis more closely. Hoffmann and co-workers[96] introduced the term *slow charge trapping* in the context of TiO_2 photocatalysis and reported diffuse reflectance IR spectroscopy (DRIFTS) data showing the decay of free and trapped electrons in polycrystalline TiO_2 after UV excitation with a high-pressure Xe lamp as light source. A broad absorption signal proportional to $\lambda^{1.7}$ (λ is the wavelength in μm) was attributed to conduction band electrons coupled to acoustic phonons of the lattice. Free carrier decay lifetimes in the range between minutes and hours were found to extend with increasing surface dehydration and dehydroxylation. Moreover, the absorption intensity of the IR active hydroxyl stretching bands is subject to the local electric fields caused by trapped electrons.[105] As a major conclusion, surface hydroxyls do actively participate in irreversible charge carrier trapping but also mediate charge recombination.[104–107]

Continued research addressing solid–gas interface effects has led to the identification of additional spectroscopic manifestations of photogenerated charges with similar UV exposure time dependent intensity changes.[13,28,97,108] *Slow charge trapping* processes have been studied in combination by using FT-IR and EPR. In addition to the IR absorption of itinerant electrons in the conduction band, trapped and localized holes (O^-) and electrons (Ti^{3+}) were measured by EPR spectroscopy.[97]

Furthermore, surface adsorbed oxygen radicals (O_2^-, O_3^-) emerging from interfacial transfer of photogenerated electrons or holes to O_2, respectively, were explored in detail on dehydroxylated TiO_2 particle surfaces.[19,28,58] In the absence of electron and hole scavengers, *i.e.* at $p < 10^{-6}$ mbar, most charge carriers recombine within a few nanoseconds.[109] Nevertheless, at cryogenic temperatures ($T \leq 140$ K) charge carrier trapping can become significant and intensity changes related to spectroscopic fingerprints can be tracked in the range of minutes to an hour. Figure 8.2 provides an illustrative example of the time-dependent increase of paramagnetic hole centers on an ensemble of TiO_2 nanocrystals as tracked by CW X-band EPR measurements. Related concentration build up reflects a steady state situation and results from a complex reaction network involving several electronic transitions that occur within a nanosecond time scale and which are typically followed by transient spectroscopies.[5,15] Observed saturation levels in intensity as well as their temperature dependence reveal important quantitative insights into materials specific factors determining the photocatalytic performance of a given material.[28,97]

During UV excitation oxygen as an electron scavenger leads to O_2 photo-adsorption and enhances the efficiency of charge separation by an order of magnitude.[28] This allows for quantification of effectively separated charge carriers per nanocrystal on the basis of volumetric titration of photo-adsorbed oxygen. Moreover, the impact of parameters such as the temperature, the energy and the flux of photons as well as the presence of hole or electron acceptors in the environmental phase can be investigated in a systematic way.

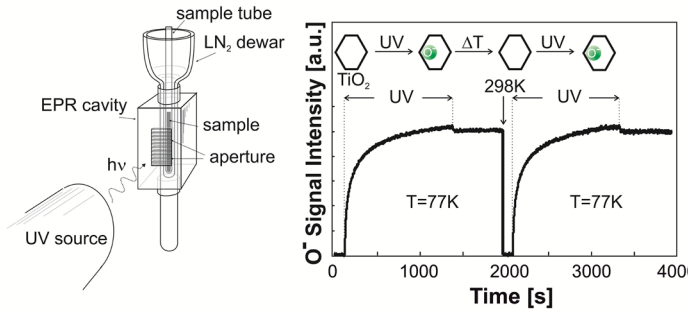

Figure 8.2 Set-up for *in situ* EPR experiments (left) and a typical time course of hole trapping (right) observed for UV excited semiconducting metal oxide nanomaterials in the temperature range $90 \leq T \leq 500$ K and at residual gas pressure of $10^{-6} \leq p \leq 10^{3}$ mbar. Typically, the EPR sample tube contains around 300 mg of a nanoparticle powder which corresponds to approximately 10^{15} TiO_2 nanocrystals. In the course of these experiments they are exposed to UV light of defined energy and photon flux.[13]

For loose powder samples, contained within a quartz glass tube at $p < 10^{-6}$ mbar and cooled *via* a liquid nitrogen reservoir (Figure 8.2, left), UV induced local heating was tracked by signal intensity changes of EPR active trapped holes.[13] Upon sample excitation with polychromatic light from a 300 W Xe lamp connected to a water filter an irradiance-independent, maximum hole center concentration $[O^-]_{max}$ corresponding to one separated electron–hole pair per particle was established at irradiances below $I = 1.55$ mW cm^{-2}. Upon light discontinuation only a minor signal intensity drop was observed with ~95% of $[O^-]_{max}$ persisting in the dark. At light irradiances $I > 1.55$ mW cm^{-2}, a secondary annihilation process for trapped holes becomes effective. This process can be tracked *in situ via* the time evolution of the O^- signal. Following an initial O^- build-up upon UV exposure a signal intensity decrease was observed and attributed to a local temperature rise and consequently an increased non-radiative recombination of electrons and holes. Upon light discontinuation sample cooling gives rise to an increase of the O^- signal intensity according to Curie's law. The contributions of enhanced electron–hole recombination and of temperature-dependent EPR sensitivity changes to the decrease of the O^- signal intensity were estimated and a local temperature increase of $\Delta T = 25$ K at $I = 6$ mW cm^{-2} was determined.

Following high intensity broad band irradiation of 300 mW cm^{-2} Howe and coworkers[27] observed a dramatic increase of the EPR signal intensity of trapped electrons once UV exposure was stopped. They postulated a light power dependent dynamic equilibrium between EPR active, trapped electrons and EPR silent conduction band electrons as the reason for the signal intensity changes observed. Local heating effects upon high intensity UV exposure, as discussed above, could also contribute to a decrease of EPR signals.

Another example for how the control over the experimental conditions (dehydroxylated and adsorbate free particle powders, cryogenic temperatures,

vacuum conditions or controlled gas atmosphere) sheds light on the impact of the materials properties on charge separation is illustrated for TiO_2 and ZrO_2 nanocrystals in Figure 8.3.[110]

Prior to the UV excitation experiments, the structure and morphology as well as the spectroscopic properties of the dehydroxylated nanoparticles were explored in detail. On this basis, the photogeneration of surface adsorbed O_2^- radicals was used to quantify the number of separated charges by EPR and to relate obtained values to the number of oxide particles that were exposed to known numbers of UV photons with defined energies. As a result, dehydroxylated ZrO_2 nanoparticles are by two orders of magnitude more efficient in oxygen-assisted charge separation than TiO_2. The diminished charge separation yield in TiO_2 was attributed to a high concentration of EPR active hole centers trapped at the particle surface. Corresponding to deep trap states these can persistently stabilize photogenerated holes and, at the same time, act as recombination centers.[110] The absence of a related defect type in ZrO_2 nanocrystals allows for a charge separation yield that is comparable to TiO_2 and compensates for the significantly wider optical band-gap (ZrO_2: 5.2 eV; TiO_2: 3.2 eV) (Figure 8.3).

Results from IR and EPR studies on dehydroxylated TiO_2 powders in high vacuum, *i.e.* at pressures below $p = 10^{-6}$ mbar,[28,39] also connect to band bending effects that are accessible to photoluminescence measurements.[108] During related studies it was found that the surface potential of TiO_2 particles alters upon UV exposure and/or upon adsorption of electron-acceptor and -donor molecules. This affects the interfacial depletion layer and, consequently, determines the depth of the active photoluminescence region. Photoluminescence is an extremely sensitive and in this context valuable tool for addressing electron–hole recombination processes upon UV exposure in conjunction with the adsorption of probe molecules.[14,108,111]

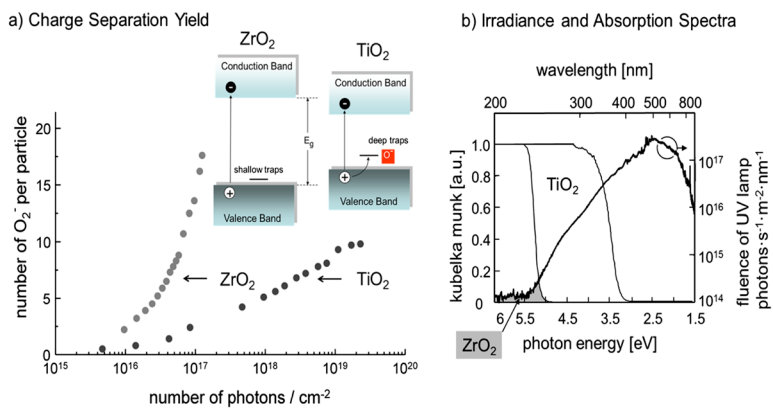

Figure 8.3 (a) Concentration of photo-adsorbed oxygen, *i.e.* number of O_2^- per particle, as a function of impinging photons corrected for the oxide specific properties of TiO_2 and ZrO_2. (b) UV absorption spectra of TiO_2 and ZrO_2 nanoparticle powders and emission spectrum of the UV source.[110]

Surface photovoltage spectroscopy (SPS) which probes light induced changes of the contact potential difference in thin films upon light exposure is a complementary non-spectroscopic approach for this type of problem.[14] Photogeneration of charge carriers and consecutive separation paths have thus been addressed in novel photocatalysts[112,113] including sensitized[114] and doped[115] semiconductors and nanocomposites.[116] Furthermore, the role of physisorbed water as a critical component of the ambient atmosphere and its effect on the redistribution of photogenerated charge carriers was addressed in a combined SPS and IR-spectroscopic approach. Water adsorbed on TiO_2 nanoparticles was proposed to induce surface states which influence the surface charge carrier redistribution.[117] Quantum mechanical calculations[101] suggest significant modifications of the density of electronic trap states upon water adsorption on anatase TiO_2 nanocrystals, and, specifically, a reduction of the number of localized states.

The evaluation of the impact of materials specific factors such as surface and interface properties on *slow charge trapping* processes on the time frame and concentration range they occur (Figure 8.2) may provide key insights to the complex and entangled mechanism that leads to the light-induced modification of macroscopic semiconductor interface properties such as the superhydrophilic behavior of TiO_2 surfaces.[118] Photoinduced as well as thermally induced interface changes have been proposed to contribute to this complex behavior, where the consumption of photogenerated charges seems to be critical.[15]

8.4 From Solid (Particle)–Gas to Solid (Particle)–Liquid Interfaces: Changes on Different Size Scales

The study of solid–liquid interfaces is far more demanding than the characterization of solid–gas or solid–vacuum interfaces. This is mainly due to the fact that the solid–liquid interfaces are buried in between two condensed phases. Surface-sensitive techniques, in turn, typically rely on the use of electrons, ions or atoms as probes. The liquid continuous phase represents a severe impediment for them. Nevertheless, a good number of approaches have now been developed as covered by a recent and insightful review.[119]

On the basis of experiments on two-dimensional model metal oxide surfaces it has been established that the structure of interfacial water, *i.e.* in the first hydration layers, is distinct from bulk water (Figure 8.4, right-hand side).[120] As identified by *in situ* X-ray scattering approaches, the organization of hydration layers is limited in extent to a few water correlation lengths. This corresponds to distances of $l \sim 1$–2 nm. Interestingly, rutile TiO_2 (110) seems to be a specific case, since a strong interaction between the first water layer and the substrate weakens the interaction of this first water layer with the subsequent ones.[121] The fact that this is not generic to all oxide surfaces underlines that the observed hydration structures are not only determined

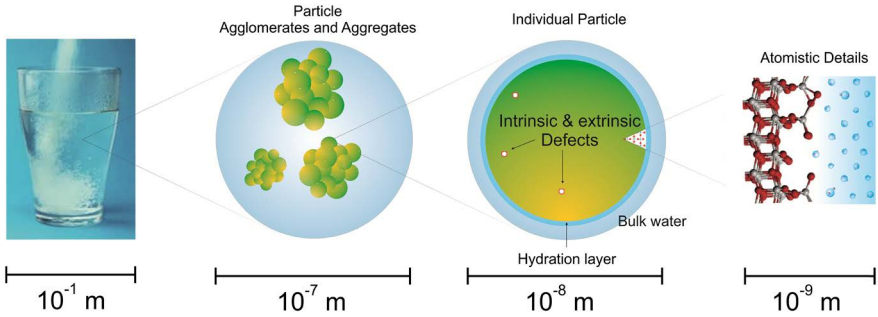

Figure 8.4 Schematic that illustrates the different lengths scales on which TiO_2 particle contact with water needs to be addressed and discussed. While surface science with support from atomistic simulations focuses on atomic scale effects (right-hand side), many charge separation effects arise from changes at the microscale, *i.e.* the change in particle assembly as mediated by the surrounding liquid continuous phase (see also Section 8.5).

by characteristics of the solid surface (*i.e.* charge, spatial arrangement and coordination of ions) but are also sensitive to the adsorption of ions out of the surrounding liquid.[121]

The high surface-to-volume ratio specific to nanoparticles corresponds to an increase in the relative fraction of surface ions. This is in line with an increase of the number of broken surface bonds relative to the bulk Ti–O bonds. Moreover, curvature effects have an impact on the relaxation of surface atoms and, thus, on their coordination geometry (Figure 8.4). Step edges and related defects serve as preferential sites for charge accumulation.[122–124] Their surface concentration is expected to increase with decreasing particle size. While nanoparticles, which are embedded in vacuum or surrounded by a fluid of chemically inert molecules, contain a fraction of isolated adsorbates, impurities and defects (Figure 8.1(b)), the properties of corresponding solid–liquid interfaces are subject to the presence of functional groups. These emerge from the interaction between coordinatively unsaturated surface ions with water and/or ions dissolved therein.[125] Terminal as well as bridging oxygen sites provide surface groups with various different protonation states (*e.g.*, $Ti–O^-$, $Ti–OH^0$, $Ti–OH_2^+$). Corresponding acid–base equilibria provide means for the pH dependent adjustment of surface charge.

With regard to metal oxide nanoparticles there exists very few systematic work which addresses the similarities and differences in the reactivity between solid–gas and solid–liquid interfaces.[126] As an interesting example, it has been found for platinum nanocrystals that the mechanisms for an alcohol oxidation reaction on the solid–gas and solid–liquid interface are entirely different. This is largely because water substantially promotes the alcohol oxidation step in the liquid and enables different and additional adsorption geometries for the species involved.[127] In other words, there are cases where condensed water molecules stabilize reaction intermediates (or photoexcited states[128,129]) and

may even facilitate the charge transfer process at the solid–liquid interfaces, while related molecules may compete with the reactants for active sites at the solid–gas interface and therefore can lower the reaction rate of the gas-phase reaction. To the best of our knowledge such comparative studies have not been pursued for TiO_2 particle systems either in the dark or under UV excitation.

For a more realistic description of the electrostatic situation of solid–liquid interfaces the shift from the concept of point charges to the charge distribution of the interfacial species has turned out to be a promising and workable concept.[125,130,131] TiO_2 nanoparticle based electrodes are employed in dye sensitized solar cells in contact with a liquid electrolyte. Electric fields were expected to be completely screened from the surface anchored dye molecules by the large dielectric constants of the semiconducting oxide and the solvent as well as the high ionic strength of the electrolyte. Transient absorption measurements, however, have shown that in the course of light-induced operation surface adsorbed sensitizer molecules in the ground state were perturbed in a way consistent with an underlying Stark effect.[132] Thus, at the TiO_2–electrolyte interface ions and solvent molecules respond to the surface electric field generated by electron injection upon reorganization from the dark equilibrium condition. Such screening effects, however, seem to be incomplete. Similar absorption changes can be induced by an electrochemical reduction of the mesoporous TiO_2 particle films, whereas the electric field experienced by the adsorbed sensitizers strongly depends on the ions in solution.[133]

Particle dispersion in liquids and their transformations into colloids generates a materials situation of substantially enhanced complexity (Figure 8.4). However, important for the investigation of charge separation, charge trapping as well as photochemistry studies, photo-electrochemistry can come into play and – in addition to its potential to quantify transferred charges – offers an additional experimental window to investigate charge redistribution effects, such as redistribution of protons inside an immobilized ensemble of TiO_2 nanoparticles (see also Sections 8.3 and 8.6).

There is a tremendous complexity increase on many length scales (Figure 8.4) when one moves from the solid *particle*–gas to the solid *particle*–liquid interface. Purely interface-specific changes that are relevant for energy and charge transfer processes as well as for adsorption and catalytic activity are typically discussed on the single particle level. However, there are also changes on the meso- or *super-particle* scale. These involve altered secondary structures of the particle ensemble (*i.e.* the state of agglomeration and aggregation) and, potentially, the generation or detachment of particle–particle interfaces.[15–17,31,134]

8.5 Microstructural Changes of Particle Ensembles and Solid–Solid Interface Formation

An important issue related to the performance of a nanoparticle-based photocatalyst is the state of particle aggregation and the nature of the interparticle forces and interfaces. While in the last few years there have been undertaken

different successful efforts to assemble TiO_2 nanoparticles into mesoporous macroscopic structures and superlattices[135–137] such as photonic crystals, nanocrystalline thin films and/or photoelectrodes to be employed for photocatalytic degradation of unwanted substances, related microstructural changes and their impact on the photo-electronic properties were scarcely addressed in a systematic way.[136,138]

Colloidal TiO_2 nanoparticle dispersions typically transform into translucent white and wet pastes when the liquid dispersing agent becomes stepwise eliminated. Finally, upon drying monolithic bulk objects with the size of millimeters and more can emerge (Figure 8.5). For reasons of simplicity and cost in the production of immobilized TiO_2 nanoparticle photo-catalysts most evaluated nanoparticle assemblies are disordered and made up from interconnected nanocrystals without any mutual orientation relationship. While in case of surface functionalized TiO_2 particle systems many disordered arrangements are homogeneous enough to enable the formation of transparent macroscopic objects,[139] this high level of organization is obviously not achieved for TiO_2 particle systems which exhibit bare particle surfaces and which are usually employed for surface and interface studies.[90]

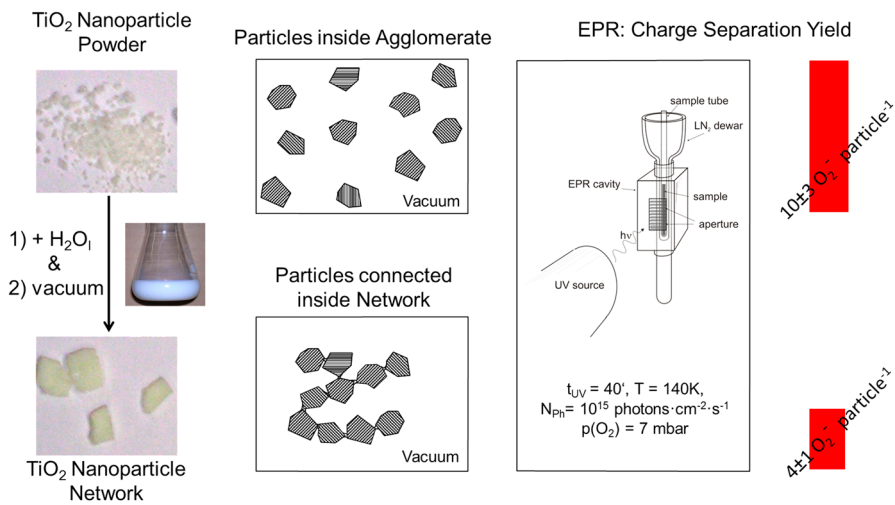

Figure 8.5 Digital images of vapor phase grown TiO_2 nanoparticle ensembles that become transformed from a powder (top) into monolithic pieces of nanoparticle aggregates (bottom) *via* intermediate contact with liquid water. The materials transformation is performed under ultrapure conditions, *i.e.* in the absence of inorganic ions, organics or surface active species. A quantitative EPR determination of the charge separation properties of the TiO_2 nanoparticle based ensemble of different microstructures revealed that solid–solid interfaces forming as a result of dehydration and dehydroxylation between the particles give rise to a significant decrease in the yield of persistently trapped charges.[140,141]

For aqueous TiO_2 nanoparticle dispersions it was actually found that aggregation reduces the generation of free hydroxyl radicals or other oxygen-based radicals.[142] First of all, related effects can be attributed to mass transfer and shadowing effects, but also electronic factors are expected to play a role. Bahnemann *et al.*[143] discovered that particular types of agglomerates enforce the electronic coupling between primary particles and – with respect to the materials' photocatalytic activity – can compensate for the concomitant loss of surface area.[142–144] Moreover, an additionally proposed mechanism relates to the rapid dissipation of photon energy.[109] Charge carrier recombination, which applies to the majority of photogenerated charge carriers within the first 100 ns, can lead to a rapid and local release of heat which breaks up the particle agglomerates and, consequently, creates for adsorption new free surface sites which were previously buried at the solid–solid interface.[15] On the other hand, opposite effects have also been reported: UV irradiation of P25 TiO_2 dispersions in water were found to lower the isoelectric point, reduce the positive surface charges and, ultimately, lead to enhanced particle aggregation and to photocatalytic activity decrease.[17] The discrepancies mentioned here clearly underline the importance of information about the surface and interface properties of TiO_2 particles in order to establish robust concepts about complex changes in the secondary structure of particle ensembles upon photoexcitation.

In the course of experiments aimed at the comparative address of solid–gas and solid–solid interface effects it was found that homogeneous nanoparticle networks show a significantly reduced capacity to separate photogenerated charges as compared to powders of isolated particles.[140] Since the intrinsic particle properties, including the chemical composition of the interface, have not been affected by the particle aggregation process itself (Figure 8.5)[31] this recombination loss must be attributed to solid–solid interfaces that facilitate the annihilation of photogenerated charges in homogeneous nanoparticle networks.[140] There are different synthetic strategies towards monolithic TiO_2 anatase nanoparticle networks available: (i) aggregation of vapor-phase grown anatase nanoparticles[31] and (ii) solution based processing of a glycolated titanium precursor combined with thermal annealing. Both approaches yield samples with high concentrations of particle–particle interfaces and comparable properties in terms of surface area, porosity and microstructure.[16] To compare the surface properties of the two types of mesoporous TiO_2 particle networks we employed paramagnetic O_2^- probes and identified the same types of surface cations as potential sites for interfacial charge transfer.[16,140] Related linkage between spectroscopically detectable defects and microstructural features represents relevant information for the rational development of mesoporous TiO_2 systems with improved efficiencies.[137,145]

Moreover, we want to point out that the processing of particle systems matters. For TiO_2 and other semiconducting metal oxides which were obtained by gas phase synthesis, it was found that the presence of water, independent of whether it is physisorbed from the surrounding ambient air or stems from

contact with liquid water, leads to the formation of solid–solid interfaces between the particles. This corresponds to the transformation of nanoparticle powders into mesoporous nanoparticle networks (Figure 8.5).[140,146] In the case of TiO_2, SnO_2 or In_2O_3 this change in microstructure and aggregation state substantially affects the optical absorption properties and the intrinsic n-type conductivity.[90,146] Such observations must be included in the evaluation of the photo-electronic properties of wet chemistry derived oxide nanostructures, such as, for example, the titania aerogels:[16,137] solvent removal as well as additional procedures aimed at bare and adsorbate free particle surfaces are inevitably associated with the production of solid–solid interfaces as highly abundant structural features with a so far unnoticed detrimental effect on the charge separation properties (Figure 8.5).[140]

From a materials' design perspective, however, the development of crystalline nanoparticle networks where the interpenetration of the different material components and the degree of compositional intermixing in the neck region of particle interfaces can be controlled is key to the rational design of photo-electronically relevant heterojunctions at the nanoscale as well as for functional particle interfaces in general.[101,141,147,148]

8.6 Charge Separation and Trapping at the Solid–Liquid Interface – Slow Processes

When a photocatalyst is in contact with a liquid electrolyte it is both the bulk and interface properties of the solid as well as electrolyte composition which determine the overall electronic structure and the potential distribution at the solid–liquid interface (Figure 8.4).[15,149–151] Upon UV excitation the electronic properties of the semiconductor–electrolyte interface then determine the branching ratio between desired charge transfer at the interface and the unwanted carrier recombination. The exploitation of photogenerated electrons and holes for the interfacial redox reactions relies on efficient charge separation that is subject to semiconductor crystal size and aggregation. For particles with dimensions larger than the space charge layer width an interfacial electric field (band bending) facilitates the transport of electrons and holes to different regions of the photocatalyst and therefore provides means for efficient charge separation.[152] In contrast, the crystal size of nanoparticles is typically too small so that band bending can be neglected. In these systems charge transport through particle agglomerates primarily occurs *via* diffusion. Charge separation, in turn, is driven by differences in the reactivity of electrons and holes towards the species available at the interface.[153]

While for free electrons and holes inside the semiconductor the potential levels of the charge carriers are determined by the conduction or valence band edges, respectively, the position of the respective band gap states sets the potential level of the trapped charge carriers. The driving force for electron- and hole-transfer processes across the semiconductor–electrolyte interface results from their position in relation to the redox potential of the

species in solution. Valence band holes in TiO_2 are characterized by a high oxidizing power (positive potentials) with respect to species at the semiconductor–electrolyte interface making oxidation reactions at the photocatalyst surface very efficient. The comparatively low reducing power of free or trapped electrons, on the other hand, is reflected by the moderately negative potential of the TiO_2 conduction band. As a consequence of the kinetic balance between the transfer of photogenerated electrons and holes, electron accumulation is typically observed in photoexcited TiO_2 catalysts, even in the presence of moderate electron acceptors such as dissolved oxygen.[154] Under such conditions electron transfer represents the rate determining step.

It was realized in the early stages of photocatalysis research that electrochemical concepts are applicable to the analysis of irradiated semiconductor particles.[4] In the case of irradiated photocatalyst particles considered as short-circuited micro-electrochemical cells and with balanced anodic and cathodic processes, the respective particle attains under irradiation a mixed photopotential which results from the relative rates of the involved oxidation and reduction reactions. At semiconductor electrodes this quantity is directly accessible *via* open circuit potential (OCP) measurements.[151] Mimicking the conditions on suspended or immobilized particles under illumination and during photocatalytic operation, the photopotential can be determined from the difference between the stationary OCP under illumination and the corresponding value measured in the dark. When under illumination photogenerated holes are preferentially transferred to solution, the OCP is more negative than in the dark due to electron accumulation in the semiconductor. Thus, the TiO_2 electrode behaves as a photoanode. Importantly, for nanocrystalline thin films a change of the electrode potential can directly be translated into a shift of the Fermi level of the photocatalyst, provided the band positions are pinned upon semiconductor charging. On this basis electrochemical and spectro-electrochemical approaches can provide direct experimental access to the density of states (DOS).[80,155–157] Moreover, open circuit photopotential decay measurements constitute a valuable tool for studying the kinetics of electron transfer and recombination reactions (Figure 8.6).[158] By using a combined approach based on voltammetric measurements in the dark and open circuit photopotential relaxation measurements on nanoporous TiO_2 thin film electrodes Monllor-Satoca *et al.*[154] determined kinetic constants at specified electron potential energies for the recombination process of electrons with trapped holes and for the reduction of oxygen molecules. In the absence of electron acceptors in solution relaxation times of the order of minutes were observed. This indicates the high stability of trapped holes at the pre-irradiated TiO_2 catalysts. Furthermore, a strong dependence of the first-order electron recombination constant on the energy or redox-potential of the electrons was observed. The latter effect was attributed to reactivity differences of trapped and quasi-free electrons. Importantly, increasing recombination constants were attributed to trapped electrons at grain boundaries.[157,159]

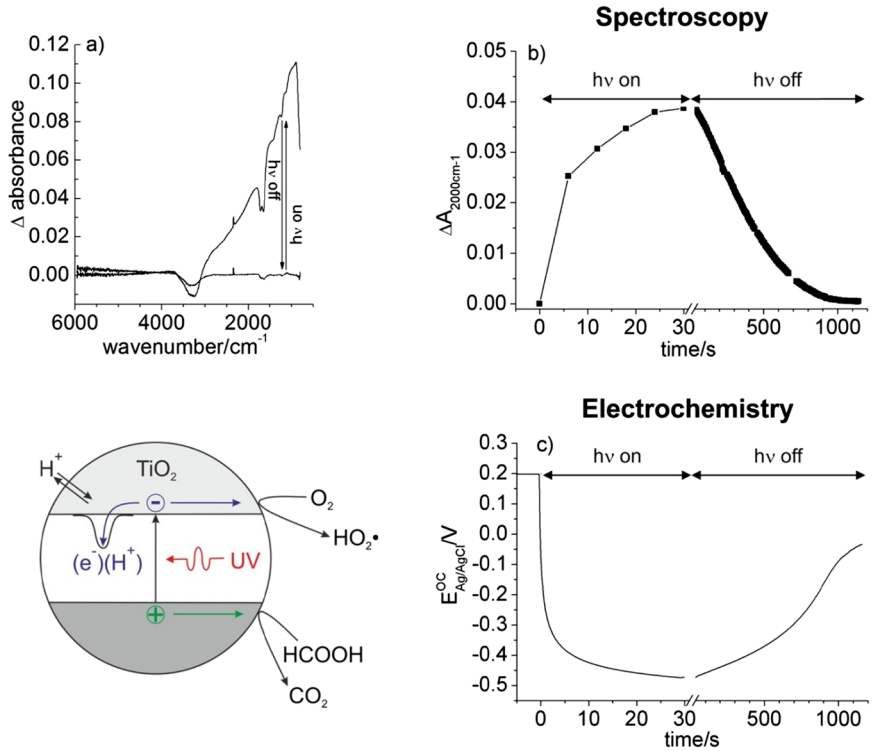

Figure 8.6 (a) IR spectra of an anatase TiO_2 nanocrystal electrode during UV exposure and after 1000 s in the dark. The reference spectra were taken prior to UV exposure at open circuit in the dark. (b) Temporal evolution of the monotonic signal (at 2000 cm^{-1}) resulting from shallow trapped electrons. (c) Open circuit potential (E^{OC}) profile measured simultaneously. Electrolyte: N_2-saturated 2 M HCOOH/0.1 M $HClO_4$ aqueous solution.[79]

The concentration and distribution of band gap states in semiconductor particles is known to critically influence the sequence of elementary reactions comprising the overall photocatalytic process. Ikeda *et al.*[160] have determined the molar amounts of defective sites in TiO_2 powders by the titration of photochemically accumulated electrons with methylviologen. The electronic energies of trap states attributed to coordinatively unsaturated Ti sites at the surface or in surface-near regions were found to be in the range of 0–0.35 V or 0–0.25 V below the conduction band edge of anatase and rutile particles, respectively. Furthermore, a linear correlation was observed between the rate constant of electron–hole recombination and the concentration of defects. Electron traps in nanostructured TiO_2 electrodes give rise to a capacitive response in electrochemical measurements which typically arises from an exponential density distribution of states below the conduction band edge. In addition, a symmetric and much weaker contribution to capacity is often observed at more positive potentials.[80,155–157,159,161–163] A comparison of the

capacitive response properties of TiO_2 thin films that consist of networks of randomly oriented nanoparticles, with those of oriented nanowire and nanotube arrays and single crystal electrodes, suggests that these deep trap states are linked to grain boundaries.[80,159] On the other hand, neither the nature or localization of the band gap states contributes to the exponential conduction band tail nor is the origin of their distribution well understood.[161] Trapping of electrons occurs presumably at various different defects in the bulk or surface regions of the mesoporous oxide and at particle–particle interfaces. But, in addition, coulombic trapping as a result of local field effects, which may originate from the interaction of electrons with the polar TiO_2 crystal or with cations of the electrolyte, could contribute to the observed distribution.[101,164] The population of band gap states in the semiconductor has an important effect on charge carrier dynamics in nanocrystalline semiconductors including the charge transfer to acceptors.[165] Zhang *et al.*[163] recently attributed a slow photocurrent response observed on TiO_2 nanotube arrays to the filling of deep traps upon UV excitation. It was shown by dynamic photocurrent measurements that the characteristic rise time of the photocurrent increases after these deep charge traps have been populated. The thermodynamic feasibility of surface reduction reactions was also found to critically depend on the energy (redox-potential) of trapped electrons. The important role of surface energetics on TiO_2 suspensions and thin films was demonstrated by Molinari *et al.*[166] who studied the reduction of a model molecule (4-nitrobenzaldehyde) bearing two functional groups of different reducibility. Mimicking reaction conditions typical for photocatalysis (*i.e.* open circuit conditions) these authors report that while the nitro group can be reduced to the amino group by electrons trapped at band gap states, potentials more negative than the flat-band potential are necessary to reduce the aldehyde to the alcohol. These consecutive reduction steps were easily tracked by open circuit potential measurements and the respective results underline that chemoselective reduction reactions can be driven at the TiO_2 surface *via* control over the energetics of the accumulated electrons.

In nanosized semiconductors that are in contact with an electrolyte solution, electrons can be accumulated not only by electrochemical polarization but also by collection of photogenerated charges. The accumulation of the negative charge is associated with charge compensation by counter ions from solution. This process corresponds to cation adsorption at the oxide surface but in principle can also lead to insertion of cations into the oxide bulk.[82,83] An important question related to the application of electrochemical methods is whether the electrochemical population of unfilled states may influence the DOS by itself.[167] This question is relevant considering the fact that upon shifting the Fermi level the potential dependent adsorption and/or cation insertion into the anatase TiO_2 lattice may alter the electronic structure of the solid.[83,168]

In some cases, negative polarization of nanocrystalline TiO_2 electrodes in aqueous electrolytes was found to enhance the photocatalytic performance of the semiconductor film.[81,169,170] This beneficial effect was attributed to

the electrochemical doping by generation of Ti^{3+} species and concomitant insertion of H^+ ions[81,169,170] or Li^+.[170] However, the extent of improvement was found to strongly depend on the nature of the electrode. Whereas only a transient improvement in mesoporous networks of differently sized nanoparticles was observed on a time scale of minutes to days a more persistent effect was obtained for arrays of TiO_2 nanotubes, the dense walls of which are composed of a nanostructured mosaic of crystallites.[171]

An enhancement of the performance in dye-sensitized solar cells was observed after visible light soaking and attributed to the formation of shallow transport levels originating from photoinduced H^+ insertion.[172] The concomitantly emerging trap states are supposed to accelerate charge carrier transport within the nanocrystalline films without deteriorating the open circuit photovoltage. In addition, H^+ insertion induced increase of the density of localized states as well as a broadening of their distribution has been claimed. Using spectro-electrochemistry Idígoras *et al.*[79,81] found that the transient electron accumulation – paralleled by proton insertion – improves both the photo-electrocatalytic and the photovoltaic properties of nanocrystalline TiO_2 electrodes. However, the persistence of charge accumulation and, consequently, the performance enhancement effect is subject to film morphology, where the higher persistence has been observed for electrodes composed of larger particles.

The reversibility of the beneficial charge accumulation prompts the question whether electrochemical doping is a true means for permanent performance improvement of nanostructured films in technological applications. Wang *et al.*[172] quite recently highlighted the analogy of light- and potential-induced improvement of the thin film performance for the case of dye-sensitized solar cells. They put proposed that *in situ* doping might occur during operation, thus substituting a repeated external modification of the electrode by cathodic polarization upon achievement of the desired performance increase. Along these lines, it was shown only recently that the occupancy of electronic states in a photocatalyst film does not depend on the type of external perturbation, if – alternatively – an external bias voltage or band gap excitation at open circuit were used to set the Fermi level position in TiO_2 based electrode.[79] More importantly, it was evidenced for the water photo-oxidation reaction that the photocatalytic performance enhancement of a TiO_2 electrode depends on the Fermi level position during electrochemical doping, rather than being dependent on the perturbation mode, *i.e.* external polarization or photoinduced electron accumulation at open circuit. Interestingly, some studies report that proton insertion may limit the performance of TiO_2 films,[173–175] as explained by factors such as Fermi level pinning, recombination enhancement or increased transport limitations.

The kinetics of the doping and the reverse process of dopant elimination following photochemical[78,79] or electrochemical charge accumulation[80] take place at a time scale of minutes to days. They can be conveniently tracked by spectroscopic and spectro-electrochemical methods, respectively, and actually correspond to *slow charge trapping processes*. Obviously, the

materials properties of the photocatalyst, in particular the doping level, not only depend on material history, *i.e.* on the synthesis and processing parameters. In addition, they are dynamic properties and may significantly change during operation. The concerted uptake of electrons and protons in a TiO_2 particle based thin film significantly alters the functional properties of the material. Clearly, knowledge of the impact of synthesis-, process- and operation-derived material properties is a prerequisite for the establishment of firm structure–property relationships. In addition to the design of more efficient photocatalysts, proton-coupled electron transfer reactions may offer a rapid and quantitative mechanism in synthetic chemistry.[176,177]

8.7 Summary and Outlook

Upon photoexcitation of TiO_2 different materials dependent and consecutive processes occur in oxide semiconductors and the nature and abundance of functional defects are determining with respect to the trapping and chemical consumption of photogenerated electrons and holes. To test hypotheses about defects as trapping sites and interface specific functionalities in heterogeneous photocatalysis it is desirable to have a system of particles with narrow distributions of size, structure and morphology.[12] This allows one to characterize the impact of various defect types – from point defects to solid–solid interfaces – on the overall electronic, chemical and optical ensemble properties. In the first part of this chapter we have seen that a strong reduction in materials complexity can be achieved when one moves from a particle with photocatalytic activity that operates in an aqueous continuous phase to a TiO_2 particle with essentially dehydroxylated and better defined surfaces and interfaces. This reduction in the complexity of materials parameters and, in particular, the increased availability of information about the surface and interface properties open the way for an unambiguous defect assignment, *i.e.* the establishment of firm links between specific spectroscopic fingerprints, on the one hand, and defects and/or functional local structures at the particle interface on the other. This is particularly true for sites which trap photogenerated charges and which have received increased attention from experimentalists and theorists performing *ab initio* calculations.

Time-dependent spectroscopy in conjunction with photoexcitation studies on semiconducting metal oxide particle systems can reveal important insights into trapping of photogenerated charges at solid–gas interfaces. For TiO_2 powders we introduced and discussed the most characteristic paramagnetic and optical fingerprints that have been identified for trapped charges and also included hydrogen impurities and associated defect states in this review. In some cases, the abundance and spectroscopic characteristics of trapping states do not depend on the gross morphology of the particle or the microstructure of the entire particle ensemble. On the other hand, we have also shown examples of microstructural transformations which can easily occur in the course of nanomaterials processing: mesoporous nanoparticle networks can emerge from solvent-mediated nanoparticle aggregation or

from the calcination of nanoparticles which previously were grown in solution. In both cases, newly formed solid–solid interfaces may give rise to very different defect related property changes, such as the enhanced recombination of photogenerated charges in semiconducting oxides.[15,16,140]

Slow charge trapping studies can track the concentration build-up of trapped charges with different extremely sensitive spectroscopies like EPR and photoluminescence in the time range between minutes and hours. This concentration build up results from the complex reaction network involving several electronic transitions that are completed within nanoseconds. Although most of these processes are investigated under experimental conditions that are far from those typically employed in photocatalysis, *i.e.* at cryogenic temperatures and in pure gas atmospheres, the obtained insights provide important information about the intrinsic particle properties, such as the beneficial or detrimental effect of dopants,[178] the impact of morphology and microstructure[7,141] and various processes inside the solid which can be studied in the absence of rate limiting mass transfer and adsorption processes at the interface. Such understanding is critical when one considers that photocatalytic particles in engineered settings, either as aqueous dispersions or deposited on substrates, are always subject to impurities as well as to the operation induced alteration of microstructures, *i.e.* size changes of aggregates upon changes of nature and strength of interparticle forces. Moreover, the exploration of *slow charge trapping* processes enables the separate characterization of adsorbed donor and acceptor species. Thus, the question of whether conclusions from photoexcitation studies, which have been carried out on model materials of reduced compositional and structural complexity, can be general enough to be linked to working catalysts in a relevant way can definitely be answered positively.

Upon contact of dry particle systems into liquid dispersing agents and their transformation into colloidal systems solid–gas interfaces are replaced by solid–liquid interfaces and the materials situation gains substantially in complexity. However, for TiO_2 particles dispersed in electrolyte solution photo-electrochemistry comes into play and – in addition to its potential to quantify transferred charges – also provides important insights into the redistribution of electrons, holes and protons inside an immobilized TiO_2 nanoparticle system.[151] In the past few decades great advances have been made in the development of novel TiO_2 based nanostructures of controlled size, shape and interface properties as model systems that are amenable to different surface and interface spectroscopies[119] in combination with photoelectrochemical techniques.[151] As demonstrated by interdisciplinary efforts in the field of TiO_2 photocatalysis, cooperation between surface science, modeling and materials science on particulate matter is key to the knowledge-based development of semiconducting oxides for photochemical applications. Related methodological advances must be transferable to other inorganic semiconductor nanostructures of comparable robustness, with controllable concentrations of functional defects and substantially improved photo-electronic and surface properties.[4]

Acknowledgements

The authors thank the German Science Foundation (DFG) for financial support through FOR 1878 (funCOS) as well as support in the framework of COST Action (CM1104) "Reducible oxide chemistry, structure and functions". We are particularly grateful to Keith McKenna, Alexander Shluger and Horst Kisch for various fruitful discussions.

References

1. A. Fujishma, X. Zhang and D. A. Tryk, *Surf. Sci. Rep.*, 2008, **63**, 515.
2. H. Kisch, *Semiconductor photocatalysis: Principles and applications*, Wiley-VCH Verlag GmbH, Weiheim, 2015.
3. J. Ryu and W. Choi, *Environ. Sci. Technol.*, 2008, **42**, 294.
4. K. Rajeshwar, A. Thomas and C. Janáky, *J. Phys. Chem. Lett.*, 2015, **6**, 139.
5. H. Kisch, *Angew. Chem., Int. Ed.*, 2013, **52**, 812.
6. D. Friedmann, C. Mendive and D. Bahnemann, *Appl. Catal., B*, 2010, **99**, 398.
7. A. Riss, M. J. Elser, J. Bernardi and O. Diwald, *J. Am. Chem. Soc.*, 2009, **131**, 6198.
8. M. A. Henderson, *Surf. Sci. Rep.*, 2011, **66**, 185.
9. U. Diebold, S.-C. Li and M. Schmid, *Annu. Rev. Phys. Chem.*, 2010, **61**, 129.
10. M. Xu, H. Noei, K. Fink, M. Muhler, Y. Wang and C. Wöll, *Angew. Chem., Int. Ed.*, 2012, **51**, 4731.
11. C. M. Friend, *Chem. Rec.*, 2014, **14**, 944.
12. T. Berger and O. Diwald, Defects at Oxide Surfaces, in *Defects in Metal Oxide Nanoparticle Powders*, ed. J. Jupille and G. Thornton, Springer International Publishing, Switzerland, 2015, vol. 58, pp. 273–301.
13. T. Berger, O. Diwald, E. Knözinger, M. Sterrer and J. T. Yates, Jr., *Phys. Chem. Chem. Phys.*, 2006, **8**, 1822.
14. Z. Zhang and J. T. Yates, *Chem. Rev.*, 2012, **112**, 5520.
15. J. Schneider, M. Matsuoka, M. Takeuchi, J. Zhang, Y. Horiuchi, M. Anpo and D. W. Bahnemann, *Chem. Rev.*, 2014, **114**, 9919.
16. S. O. Baumann, M. J. Elser, M. Auer, J. Bernardi, N. Hüsing and O. Diwald, *Langmuir*, 2011, **27**, 1946.
17. J. Sun, L.-H. Guo, H. Zhang and L. Zhao, *Environ. Sci. Technol.*, 2014, **48**, 11962.
18. T. L. Thompson and J. T. Yates Jr, *Chem. Rev.*, 2006, **106**, 4428.
19. E. Carter, A. F. Carley and D. M. Murphy, *J. Phys. Chem. C*, 2007, **111**, 10630.
20. Z. Wang, W. Ma, C. Chen, H. Ji and J. Zhao, *Chem. Eng. J.*, 2011, **170**, 353.
21. S. van Doorslaer and D. M. Murphy, *Top. Curr. Chem.*, 2012, **321**, 1.
22. R. F. Howe and M. Grätzel, *J. Phys. Chem.*, 1985, **89**, 4495.
23. T. Berger, M. Sterrer, O. Diwald and E. Knözinger, *ChemPhysChem*, 2005, **6**, 2104.

24. D. C. Hurum, A. G. Agrios, S. E. Crist, K. A. Gray, T. Rajh and M. C. Thurnauer, *J. Electron Spectrosc. Relat. Phenom.*, 2006, **150**, 155.
25. G. Li, N. M. Dimitrijevic, L. Chen, J. M. Nichols, T. Rajh and K. A. Gray, *J. Am. Chem. Soc.*, 2008, **130**, 5402.
26. M. Chiesa, E. Giamello and M. Che, *Chem. Rev.*, 2010, **110**, 1320.
27. I. R. MacDonald, S. Rhydderch, E. Holt, N. Grant, J. M. D. Storey and R. F. Howe, *Catal. Today*, 2012, **182**, 39.
28. T. Berger, M. Sterrer, O. Diwald and E. Knözinger, *ChemPhysChem*, 2005, **6**, 2104.
29. C. Naccache, P. Meriaudeau, M. Che and A. J. Tench, *Trans. Faraday Soc.*, 1971, **67**, 506.
30. M. Chiesa, M. C. Paganini, S. Livraghi and E. Giamello, *Phys. Chem. Chem. Phys.*, 2013, **15**, 9435.
31. M. J. Elser, T. Berger, D. Brandhuber, J. Bernardi, O. Diwald and E. Knözinger, *J. Phys. Chem. B*, 2006, **110**, 7605.
32. M. Che and A. J. Tench, *Adv. Catal.*, 1982, **31**, 77.
33. A. L. Attwood, D. M. Murphy, J. L. Edwards, T. A. Egerton and R. W. Harrison, *Res. Chem. Intermed.*, 2003, **29**, 449.
34. A. M. Volodin, A. E. Cherkashin and V. S. Zakharenko, *React. Kinet. Catal. Lett.*, 1979, **11**, 103.
35. M. Che and A. J. Tench, *Adv. Catal.*, 1983, **32**, 1.
36. Z. Zhang and J. T. Yates Jr, *J. Am. Chem. Soc.*, 2010, **132**, 12804.
37. M. Anpo, Y. Kubokawa, T. Fujii and S. Suzuki, *J. Phys. Chem.*, 1984, **88**, 2572.
38. T. Rajh, A. E. Ostafin, O. I. Micic, D. M. Tiede and M. C. Thurnauer, *J. Phys. Chem.*, 1996, **100**, 4538.
39. T. Berger, O. Diwald, E. Knözinger, F. Napoli, M. Chiesa and E. Giamello, *Chem. Phys.*, 2007, **339**, 138.
40. A. T. Brant, N. C. Giles, S. Yang, M. A. R. Sarker, S. Watauchi, M. Nagao, I. Tanaka, D. A. Tryk, A. Manivannan and L. E. Halliburton, *J. Appl. Phys.*, 2013, **114**, 113702.
41. M. Nolan, S. Elliott, J. Mulley, R. Bennett, M. Basham and P. Mulheran, *Phys. Rev. B*, 2008, **77**, 235424.
42. P. Deák, B. Aradi and T. Frauenheim, *Phys. Rev. B*, 2012, **86**, 195206.
43. C. Di Valentin and G. Pacchioni, *Acc. Chem. Res.*, 2014, **47**, 3233.
44. F. D. Brandão, M. V. B. Pinheiro, G. M. Ribeiro, G. Medeiros-Ribeiro and K. Krambrock, *Phys. Rev. B*, 2009, **80**, 235204.
45. Y. Wang, C. Feng, M. Zhang, J. Yang and Z. Zhang, *Appl. Catal., B*, 2010, **100**, 84.
46. B. Choudhury and A. Choudhury, *Sci. Adv. Mater.*, 2014, **6**, 2115.
47. E. Serwicka, M. Schlierkamp and R. Schindler, *Z. Naturforsch.*, 1981, **36**, 226.
48. S. Horikoshi, Y. Minatodani, H. Tsutsumi, H. Uchida, M. Abe and N. Serpone, *J. Photochem. Photobiol., A*, 2013, **265**, 20.
49. V. N. Kuznetsov and N. Serpone, *J. Phys. Chem. C*, 2009, **113**(34), 15110.

50. V. V. Titov, R. V. Mikhaylov and A. A. Lisachenko, *J. Phys. Chem. C*, 2014, **118**, 21986.
51. Y. Chen, X. Cao, B. Lin and B. Gao, *Appl. Surf. Sci.*, 2013, **264**, 845.
52. O. F. Schirmer, *J. Phys.: Condens. Matter*, 2006, **18**, R667.
53. P. Zawadzki, *J. Phys. Chem. C*, 2013, **117**, 8647.
54. M. Grätzel and R. F. Howe, *J. Phys. Chem.*, 1990, **94**, 2566.
55. A. M. Volodin, S. E. Malykhin and G. M. Zhidomirov, *Kinet. Catal.*, 2011, **52**, 605.
56. A. M. Volodin, *Catal. Today*, 2000, **58**, 103.
57. V. Brezová, Z. Barbieriková, M. Zukalová, D. Dvoranová and L. Kavan, *Catal. Today*, 2014, **230**, 112.
58. A. L. Attwood, J. L. Edwards, C. C. Rowlands and D. M. Murphy, *J. Phys. Chem. A*, 2003, **107**, 1779.
59. M. Brustolon and E. Giamello, *Electron Paramagnetic Resonance: A Practitioner's Toolkit*, John Wiley & Sons, Inc., Hoboken, NJ, 2009.
60. Y. Nosaka, S. Komori, K. Yawata, T. Hirakawa and A. Y. Nosaka, *Phys. Chem. Chem. Phys.*, 2003, **5**, 4731.
61. C. G. van de Walle, *Phys. Rev. Lett.*, 2000, **85**, 1012.
62. M. D. McCluskey, M. C. Tarun and S. T. Teklemichael, *J. Mater. Res.*, 2012, **27**, 2190.
63. C. Di Valentin, G. Pacchioni and A. Selloni, *J. Phys. Chem. C*, 2009, **113**, 20543.
64. W. M. Hlaing Oo, S. Tabatabaei, M. D. McCluskey, J. B. Varley, A. Janotti and C. G. Van de Walle, *Phys. Rev. B*, 2010, **82**, 193201.
65. F. Bekisli, M. Stavola, W. B. Fowler, L. Boatner, E. Spahr and G. Lüpke, *Phys. Rev. B*, 2011, **84**, 035213.
66. H. Noei, H. Qiu, Y. Wang, M. Muhler and C. Wöll, *ChemPhysChem*, 2010, **11**, 3604.
67. H. Sezen, M. Buchholz, A. Nefedov, C. Natzeck, S. Heissler, C. Di Valentin and C. Wöll, *Sci. Rep.*, 2014, **4**, 3808.
68. G. Ghiotti, A. Chiorino and F. Boccuzzi, *Surf. Sci.*, 1993, **287–288**, 228.
69. F. Boccuzzi, E. Guglielminotti and A. Chiorino, *Sens. Actuators, B*, 1992, **7**, 645.
70. C. A. Wolden, T. M. Barnes, J. B. Baxter and E. S. Aydil, *J. Appl. Phys.*, 2005, **97**, 043522.
71. F. Traeger, M. Kauer, C. Wöll, D. Rogalla and H.-W. Becker, *Phys. Rev. B*, 2011, **84**, 075462.
72. D. A. Panayotov, S. P. Burrows, J. T. Yates and J. R. Morris, *J. Phys. Chem. C*, 2011, **115**, 22400.
73. D. A. Panayotov, S. P. Burrows and J. R. Morris, *J. Phys. Chem. C*, 2012, **116**, 4535.
74. J. Biedrzycki, S. Livraghi, E. Giamello, S. Agnoli and G. Granozzi, *J. Phys. Chem. C*, 2014, **118**, 8462.
75. X.-L. Yin, M. Calatayud, H. Qiu, Y. Wang, A. Birkner, C. Minot and C. Wöll, *ChemPhysChem*, 2008, **9**, 253.

76. M. M. Islam, M. Calatayud and G. Pacchioni, *J. Phys. Chem. C*, 2011, **115**, 6809.
77. J. Tao, Q. Cuan, X.-Q. Gong and M. Batzill, *J. Phys. Chem. C*, 2012, **116**, 20438.
78. D. M. Savory and A. James McQuillan, *J. Phys. Chem. C*, 2014, **118**, 13680.
79. T. Berger and J. A. Anta, *Anal. Chem.*, 2012, **84**, 3053.
80. T. Berger, J. A. Anta and V. Morales-Flórez, *J. Phys. Chem. C*, 2012, **116**, 11444.
81. J. Idígoras, T. Berger and J. A. Anta, *J. Phys. Chem. C*, 2013, **117**, 1561.
82. B. I. Lemon and J. T. Hupp, *J. Phys. Chem.*, 1996, **100**(35), 14578.
83. L. A. Lyon and J. T. Hupp, *J. Phys. Chem. B*, 1999, **103**, 4623.
84. V. Spagnol, E. Sutter, C. Debiemme-Chouvy, H. Cachet and B. Baroux, *Electrochim. Acta*, 2009, **54**, 1228.
85. G. Rothenberger, J. Moser, M. Grätzel, N. Serpone and D. K. Sharma, *J. Am. Chem. Soc.*, 1985, **107**, 8054.
86. I. A. Shkrob and M. C. Sauer Jr, *J. Phys. Chem. B*, 2004, **108**, 12497.
87. T. Yoshihara, R. Katoh, A. Furube, Y. Tamaki, M. Murai, K. Hara, S. Murata, H. Arakawa and M. Tachiya, *J. Phys. Chem. B*, 2004, **108**, 3817.
88. A. I. Kuznetsov, O. Kameneva, A. Alexandrov, N. Bityurin, P. Marteau, K. Chhor, C. Sanchez and A. Kanaev, *Phys. Rev. E*, 2005, **71**, 021403.
89. A. A. Lisachenko, V. N. Kuznetsov, M. N. Zakharov and R. V. Mikhailov, *Kinet. Catal.*, 2004, **45**, 189.
90. M. J. Elser and O. Diwald, *J. Phys. Chem. C*, 2012, **116**, 2896.
91. A. Safrany, R. Gao and J. Rabani, *J. Phys. Chem. B*, 2000, **104**, 5848.
92. B. O'Regan, M. Grätzel and D. Fitzmaurice, *Chem. Phys. Lett.*, 1991, **183**, 89.
93. F. Cao, G. Oskam, P. C. Searson, J. M. Stipkala, T. A. Heimer, F. Farzad and G. J. Meyer, *J. Phys. Chem.*, 1995, **99**, 11974.
94. V. M. Khomenko, K. Langer, H. Rager and A. Fett, *Phys. Chem. Miner.*, 1998, **25**, 338.
95. G. Boschloo and D. Fitzmaurice, *J. Phys. Chem. B*, 1999, **103**, 7860.
96. S. H. Szczepankiewicz, J. A. Moss and M. R. Hoffmann, *J. Phys. Chem. B*, 2002, **106**, 2922.
97. T. Berger, M. Sterrer, O. Diwald, E. Knözinger, D. Panayotov, T. L. Thompson and J. T. Yates, Jr, *J. Phys. Chem. B*, 2005, **109**, 6061.
98. D. A. Panayotov and J. T. Yates, Jr, *Chem. Phys. Lett.*, 2007, **436**, 204.
99. D. A. Panayotov and J. T. Yates, Jr, *J. Phys. Chem. C*, 2007, **111**, 2959.
100. T. Ohno, K. Sarukawa and M. Matsumura, *New J. Chem.*, 2002, **26**, 1167.
101. F. Nunzi, E. Mosconi, L. Storchi, E. Ronca, A. Selloni, M. Grätzel and F. de Angelis, *Energy Environ. Sci.*, 2013, **6**, 1221.
102. S. K. Wallace and K. P. McKenna, *J. Phys. Chem. C*, 2015, **119**, 1913.
103. B. Liu and X. Zhao, *Phys. Chem. Chem. Phys.*, 2014, **16**, 22343.
104. M. H. Rittmann-Frank, C. J. Milne, J. Rittmann, M. Reinhard, T. J. Penfold and M. Chergui, *Angew. Chem., Int. Ed.*, 2014, **53**, 5858.
105. S. H. Szczepankiewicz, J. A. Moss and M. R. Hoffmann, *J. Phys. Chem. B*, 2002, **106**, 7654.

106. M. A. Henderson, W. S. Epling, C. H. F. Peden and C. L. Perkins, *J. Phys. Chem. B*, 2003, **107**, 534.
107. M. A. Henderson, J. M. White, H. Uetsuka and H. Onishi, *J. Am. Chem. Soc.*, 2003, **125**, 14974.
108. A. Stevanovic, M. Büttner, Z. Zhang and J. T. Yates, Jr, *J. Am. Chem. Soc.*, 2012, **134**, 324.
109. S. Leytner and J. T. Hupp, *Chem. Phys. Lett.*, 2000, **330**, 231.
110. N. Siedl, M. J. Elser, E. Halwax, J. Bernardi and O. Diwald, *J. Phys. Chem. C*, 2009, **113**, 9175.
111. A. Stevanovic and J. T. Yates, Jr, *Langmuir*, 2012, **28**, 5652.
112. F. A. Frame, T. K. Townsend, R. L. Chamousis, E. M. Sabio, T. Dittrich, N. D. Browning and F. E. Osterloh, *J. Am. Chem. Soc.*, 2011, **133**, 7264.
113. J. Zhao and F. E. Osterloh, *J. Phys. Chem. Lett.*, 2014, **5**, 782.
114. P. Zabel, T. Dittrich, M. Funes, E. N. Durantini and L. Otero, *J. Phys. Chem. C*, 2009, **113**, 21090.
115. R. Beranek, B. Neumann, S. Sakthivel, M. Janczarek, T. Dittrich, H. Tributsch and H. Kisch, *Chem. Phys.*, 2007, **339**, 11.
116. P. Luan, M. Xie, D. Liu, X. Fu and L. Jing, *Sci. Rep.*, 2014, **4**, 6180.
117. D. S. Warren, Y. Shapira, H. Kisch and A. J. Mcquillan, *J. Phys. Chem. C*, 2007, **111**, 14286.
118. R. Wang, K. Hashimoto, A. Fujishima, M. Chikuni, E. Kojima, A. Kitamura, M. Shimohigoshi and T. Watanabe, *Nature*, 1997, **388**, 431.
119. F. Zaera, *Chem. Rev.*, 2012, **112**, 2920.
120. P. Fenter and S. S. Lee, *MRS Bull.*, 2014, **39**, 1056.
121. Z. Zhang, P. Fenter, L. Cheng, N. C. Sturchio, M. J. Bedzyk, M. Předota, A. Bandura, J. D. Kubicki, S. N. Lvov, P. T. Cummings, A. A. Chialvo, M. K. Ridley, P. Bénézeth, L. Anovitz, D. A. Palmer, M. L. Machesky and D. J. Wesolowski, *Langmuir*, 2004, **20**, 4954.
122. U. Martinez, J. Ø. Hansen, E. Lira, H. H. Kristoffersen, P. Huo, R. Bechstein, E. Lægsgaard, F. Besenbacher, B. Hammer and S. Wendt, *Phys. Rev. Lett.*, 2012, **109**, 155501.
123. M. Setvin, X. Hao, B. Daniel, J. Pavelec, Z. Novotny, G. S. Parkinson, M. Schmid, G. Kresse, C. Franchini and U. Diebold, *Angew. Chem., Int. Ed.*, 2014, **53**, 4714.
124. H. Takahashi, R. Watanabe, Y. Miyauchi and G. Mizutani, *J. Chem. Phys.*, 2011, **134**, 154704.
125. K. Bourikas, C. Kordulis and A. Lycourghiotis, *Chem. Rev.*, 2014, **114**, 9754.
126. B. L. Mojet, S. D. Ebbesen and L. Lefferts, *Chem. Soc. Rev.*, 2010, **39**, 4643.
127. H. Wang, A. Sapi, C. M. Thompson, F. Liu, D. Zherebetskyy, J. M. Krier, L. M. Carl, X. Cai, L.-W. Wang and G. A. Somorjai, *J. Am. Chem. Soc.*, 2014, **136**, 10515.
128. K. Onda, B. Li, J. Zhao, K. D. Jordan, J. Yang and H. Petek, *Science*, 2005, **308**, 1154.
129. H. Petek and J. Zhao, *Chem. Rev.*, 2010, **110**, 7082.

130. T. Hiemstra, J. de Wit and W. van Riemsdijk, *J. Colloid Interface Sci.*, 1989, **133**, 105.
131. T. Hiemstra and W. H. Van Riemsdijk, *J. Colloid Interface Sci.*, 1999, **210**, 182.
132. S. Ardo, Y. Sun, A. Staniszewski, F. N. Castellano and G. J. Meyer, *J. Am. Chem. Soc.*, 2010, **132**, 6696.
133. R. M. O'Donnell, S. Ardo and G. J. Meyer, *J. Phys. Chem. Lett.*, 2013, **4**, 2817.
134. C.-y. Wang, C. Böttcher, D. W. Bahnemann and J. K. Dohrmann, *J. Nanopart. Res.*, 2004, **6**, 119.
135. D. Fattakhova-Rohlfing, A. Zaleska and T. Bein, *Chem. Rev.*, 2014, **114**, 9487.
136. Y. Chen, F. Huang, W. Xiang, D. Chen, L. Cao, L. Spiccia, R. A. Caruso and Y.-B. Cheng, *Nanoscale*, 2014, **6**, 13787.
137. T. Fröschl, U. Hörmann, P. Kubiak, G. Kučerová, M. Pfanzelt, C. K. Weiss, R. J. Behm, N. Hüsing, U. Kaiser, K. Landfester and M. Wohlfahrt-Mehrens, *Chem. Soc. Rev.*, 2012, **41**, 5313.
138. E. M. Hotze, J.-Y. Bottero and M. R. Wiesner, *Langmuir*, 2010, **26**, 11170.
139. D. Koziej, A. Lauria and M. Niederberger, *Adv. Mater.*, 2014, **26**, 235.
140. N. Siedl, M. J. Elser, J. Bernardi and O. Diwald, *J. Phys. Chem. C*, 2009, **113**, 15792.
141. N. Siedl, S. O. Baumann, M. J. Elser and O. Diwald, *J. Phys. Chem. C*, 2012, **116**, 22967.
142. D. Jassby, J. Farner Budarz and M. Wiesner, *Environ. Sci. Technol.*, 2012, **46**, 6934.
143. C.-Y. Wang, C. Böttcher, D. W. Bahnemann and J. K. Dohrmann, *J. Mater. Chem.*, 2003, **13**, 2322.
144. M. Che and J. C. Védrine, *Characterization of Solid Materials and Heterogeneous Catalysts: From Structure to Surface Reactivity*, Wiley-VCH Verlag GmbH, Weinheim, 2012.
145. R. Zhang, A. A. Elzatahry, S. S. Al-Deyab and D. Zhao, *Nano Today*, 2012, **7**, 344.
146. N. Siedl, P. Gügel and O. Diwald, *Langmuir*, 2013, **29**, 6077.
147. T. Xia, N. Li, Y. Zhang, M. B. Kruger, J. Murowchick, A. Selloni and X. Chen, *ACS Appl. Mater. Interfaces*, 2013, **5**, 9883.
148. R. Marschall, *Adv. Funct. Mater.*, 2014, **24**, 2421.
149. A. Natarajan, G. Oskam and P. C. Searson, *J. Phys. Chem. B*, 1998, **102**, 7793.
150. D. Vanmaekelbergh, A. J. Houtepen and J. J. Kelly, *Electrochim. Acta*, 2007, **53**, 1140.
151. T. Berger, D. Monllor-Satoca, M. Jankulovska, T. Lana-Villarreal and R. Gómez, *ChemPhysChem*, 2012, **13**, 2824.
152. A. Hagfeldt and M. Grätzel, *Chem. Rev.*, 1995, **95**, 49.
153. P. V. Kamat, K. Tvrdy, D. R. Baker and J. G. Radich, *Chem. Rev.*, 2010, **110**, 6664.
154. D. Monllor-Satoca and R. Gómez, *J. Phys. Chem. C*, 2008, **112**, 139.

155. L. Kavan, K. Kratochvilová and M. Grätzel, *J. Electroanal. Chem.*, 1995, **394**, 93.
156. J. Bisquert, F. Fabregat-Santiago, I. Mora-Seró, G. Garcia-Belmonte, E. M. Barea and E. Palomares, *Inorg. Chim. Acta*, 2008, **361**, 684.
157. T. Berger, T. Lana-Villarreal, D. Monllor-Satoca and R. Gómez, *J. Phys. Chem. C*, 2007, **111**, 9936.
158. K. Vinodgopal, S. Hotchandani and P. V. Kamat, *J. Phys. Chem.*, 1993, **97**, 9040.
159. M. Jankulovska, T. Berger, S. S. Wong, R. Gómez and T. Lana-Villarreal, *ChemPhysChem*, 2012, **13**, 3008.
160. S. Ikeda, N. Sugiyama, S.-y. Murakami, H. Kominami, Y. Kera, H. Noguchi, K. Uosaki, T. Torimoto and B. Ohtani, *Phys. Chem. Chem. Phys.*, 2003, **5**, 778.
161. L. Bertoluzzi, I. Herraiz-Cardona, R. Gottesman, A. Zaban and J. Bisquert, *J. Phys. Chem. Lett.*, 2014, **5**, 689.
162. M. Jankulovska, T. Berger, T. Lana-Villarreal and R. Gómez, *Electrochim. Acta*, 2012, **62**, 172.
163. Q. Zhang, V. Celorrio, K. Bradley, F. Eisner, D. Cherns, W. Yan and D. J. Fermín, *J. Phys. Chem. C*, 2014, **118**, 18207.
164. L. Peter, *Acc. Chem. Res.*, 2009, **42**, 1839.
165. J. Bisquert, *Phys. Chem. Chem. Phys.*, 2008, **10**, 49.
166. A. Molinari, A. Maldotti and R. Amadelli, *Chem.–Eur. J.*, 2014, **20**, 7759.
167. A. J. Morris and G. J. Meyer, *J. Phys. Chem. C*, 2008, **112**, 18224.
168. G. Boschloo and D. Fitzmaurice, *J. Phys. Chem. B*, 1999, **103**, 2228.
169. T. Berger, T. Lana-Villarreal, D. Monllor-Satoca and R. Gómez, *Electrochem. Commun.*, 2006, **8**, 1713.
170. B. H. Meekins and P. V. Kamat, *ACS Nano*, 2009, **3**, 3437.
171. O. K. Varghese, D. Gong, M. Paulose, C. A. Grimes and E. C. Dickey, *J. Mater. Res.*, 2003, **18**, 156.
172. Q. Wang, Z. Zhang, S. M. Zakeeruddin and M. Grätzel, *J. Phys. Chem. C*, 2008, **112**, 7084.
173. F. Fabregat-Santiago, E. M. Barea, J. Bisquert, G. K. Mor, K. Shankar and C. A. Grimes, *J. Am. Chem. Soc.*, 2008, **130**, 11312.
174. A. F. Halverson, K. Zhu, P. T. Erslev, J. Y. Kim, N. R. Neale and A. J. Frank, *Nano Lett.*, 2012, **12**, 2112.
175. J. R. Swierk, N. S. McCool, T. P. Saunders, G. D. Barber and T. E. Mallouk, *J. Am. Chem. Soc.*, 2014, **136**, 10974.
176. J. N. Schrauben, R. Hayoun, C. N. Valdez, M. Braten, L. Fridley and J. M. Mayer, *Science*, 2012, **336**, 1298.
177. C. N. Valdez, M. Braten, A. Soria, D. R. Gamelin and J. M. Mayer, *J. Am. Chem. Soc.*, 2013, **135**, 8492.
178. M. D'Arienzo, N. Siedl, A. Sternig, R. Scotti, F. Morazzoni, J. Bernardi and O. Diwald, *J. Phys. Chem. C*, 2010, **114**, 18067.